Nanopore ion sources deliver single amino acid and peptide ions directly into high vacuum

Nicholas Drachman[1], Mathilde LePoitevin[1], Hannah Szapary[1], Benjamin Wiener[1], William Maulbetsch[1] and Derek Stein[1,2]

[1]Physics Department, Brown University, 182 Hope street, Providence, 02906, RI, USA.
[2]School of Engineering, Brown University, 184 Hope street, Providence, 02906, RI, USA.

Abstract

We report a nanopore ion source for mass spectrometry that delivers ions directly into high vacuum from aqueous solutions. The ion source comprises a pulled quartz capillary with a sub-100 nm opening. Ions escape an electrified meniscus between the liquid and high vacuum by ion evaporation and travel along collisionless trajectories to the ion detector. We measure mass spectra of 16 different amino acid ions as well as post-translationally modified variants of glutathione in unsolvated states using the nanopore ion source. The emitted current is composed of ions rather than charged droplets, and more than 90% of the current can be recovered in a distant collector. The nanopore ion source could enable more sensitive proteomic analyses. It circumvents the sample loss mechanisms inherent to conventional electrospray ionization (ESI), where charged droplets are sprayed into a background gas that scatters ions and degrades their transmission.

Keywords: proteomics, nanopore, mass spectrometry, ion source, single molecule

1 Introduction

Mass spectrometry (MS) is the workhorse of proteomics research thanks to its ability to distinguish amino acids and small peptides by their mass [1]. Its utility also significantly derives from the availability of soft ionization techniques for transferring peptide ions into the gas phase intact [2]. In particular, electropray ionization (ESI) transfers analyte into a mass spectrometer via a plume of charged droplets that emerge from a liquid cone-jet at the end of a voltage-biased capillary, as illustrated in Fig. 1a [3]. The droplets pass through a background gas that induces a string of evaporation and Coulomb explosion cycles that ultimately release analyte ions into the gas phase [4]. However, the background gas needed to liberate ions from droplets is also a source of significant sample loss that limits the sensitivity of MS.

The background gas and the plume of charged droplets it creates widely disperse ions, the majority of which collide with the transfer capillary, which bridges the ambient-pressure ion source and the first pumping stage of the mass spectrometer, or other hardware components upstream of the detector [2]. Early ESI sources had emitter tips with diameters of hundreds of micrometers, and only one ion in $\sim 10^4$ reached the mass analyzer [5]. Nano-electrospray ionization (nano-ESI) increased the ion transmission efficiency to $\sim 1\%$ in typical measurements (occasionally reaching as high as 12%) by using emitters with micrometer-scale tips that reduced the flow rates to the range of several nL/min [6–8]. Marginean *et al.* demonstrated that by optimizing the background gas pressure, the sheath gas flow rate, and the ion funnel voltages of a subambient pressure nano-ESI source, they could achieve an ion utilization efficiency (the fraction of analyte originally in solution reaching the detector) as high as 50% for neurotensin [9]. However, co-optimizing the efficiency of

multiple analytes is fundamentally challenging because ESI involves processes that physically separate different ion species within the plume [10]. State-of-the-art MS instrumentation still requires thousands to millions of copies of proteins for their identification [11, 12]. This sensitivity falls short of what is desired for single-cell proteomics and single molecule analyses [13–15]. Achieving single-molecule sensitivity requires an ion source that circumvents the loss mechanisms from spraying charged droplets into a background gas.

We have developed a nanopore ion source that emits amino acid and small peptide ions directly into high vacuum from its tip (Fig. 1b). The heart of the ion source is a pulled quartz capillary with a tip whose inner tip diameter is smaller than 100 nm [16]. We reason that the smallness of the tip will influence ion emission in three important ways: First, the surface tension of water can maintain a stable liquid-vacuum interface that supports many atmospheres of pressure when stretched across a nanoscale opening. Second, the fluid flow rate, which scales as the inverse cube of the tip diameter, is too low for a stable electrospray cone-jet to form [17, 18], and this may prevent charged droplets from being emitted altogether. Third, electric fields will concentrate at a sharp, conductive tip like an electrolyte-filled nanocapillary, reach ~ 1 V/nm at the meniscus [19], and draw out ions at high rates by the process of ion evaporation [20].

Here we characterize the emission of ions by a nanopore ion source from aqueous solution directly into high vacuum. We obtain mass spectra of amino acids and small peptides using a custom quadrupole mass spectrometer [21] in which the nanopore ion source operates at pressures below 10^{-6} torr (Fig. 1c). Separately, we measure greater than 93% transmission of current between an

electrolyte filled ion source and a downstream Faraday cup. We further separate the contributions of charged droplets and ions to the tip current using a magnetic sector and thereby demonstrate that the nanopore ion source can be made to emit only ions. The significance of this study is the simplicity with which the nanopore ion source efficiently transfers ions into high vacuum without the complications of conventional ESI, such as ion funnels, multiple pumping stages, transfer capillaries, and droplet plumes.

2 Results

2.1 Emitting amino acid ions from a nanopore ion source

We characterize the emission of amino acids from aqueous solution in a custom quadrupole mass spectrometer shown in Fig. 1c [21]. In a typical experiment, ion emission from a nanopore ion source is initiated by applying an extraction voltage, V_E, in the range +260 V to +360 V between the tip and the extraction electrode. This range of V_E is significantly lower than the voltages typically needed to initiate electrospray in conventional ESI or nano-ESI sources [2]. The tip current, I_T, is typically in the range of 3-20 pA. The onset of current is abrupt and usually accompanied by the measurement of ions striking the instrument's detector. We collect easily interpretable mass spectra within minutes at these low tip currents.

Fig. 1d shows the mass spectrum of a 100 mM solution of arginine in water. This spectrum is obtained in positive ion mode using a nanopore ion source with inner tip diameter of 41 nm. Five peaks are clearly visible. The peak at 175 m/z corresponds to the singly charged arginine ion (Arg^+). The higher

m/z peaks are all separated by 18 m/z, the shift induced by an additional water molecule. Thus, the other peaks correspond to solvated states of arginine ($Arg^+(H_2O)_n$), where the solvation number n ranges from 1 to 4.

Figure 2a illustrates how the tip diameter influences arginine mass spectra. The spectra shown are obtained using nanocapillaries with inner tip diameters of 20 nm, 125 nm, and 300 nm. The largest tip produces a broad spectrum of peaks that includes the bare arginine ion, eight incrementally hydrated arginine ion clusters, and a peak at 349 m/z that corresponds to the arginine dimer ion $(Arg{\cdot}Arg + H)^+$. The intermediate-sized tip produces a narrower spectrum that includes the bare arginine ion, six incrementally hydrated arginine ion clusters, and a relatively diminished arginine dimer ion peak. The smallest tip primarily produces the bare arginine ion, but attenuated peaks corresponding to the singly and doubly hydrated arginine ion clusters are also visible in the spectrum. Smaller tips tend to produce relatively stronger signals and less noisy spectra than larger tips, as can be seen by comparing the baselines of the three spectra in Fig. 2a. We observe some variance in the distribution of solvation states between nanocapillaries with similar tip sizes (e.g., compare the spectrum in Fig. 1d produced by a 41 nm tip to the spectrum from Fig. 2a produced by a 20 nm tip). However, only nanocapillaries with inner tip diameters smaller than about 65 nm have produced spectra where most of the amino acid ions are measured in the unsolvated state.

Figure 2b shows mass spectra obtained from 16 different aqueous amino acid solutions, all at 100 mM concentration with the exception of Tryptophan which was 50 mM. Four different nanopocapillaries with inner tip diameters of 20, 25, 57 and 58 nm were used for these measurements. The most prominent amino acid peak in every spectrum shown in Fig. 2b corresponds to a

singly charged and unsolvated ion. The spectra for glycine, alanine, proline, valine, cysteine, glutamine, and phenylalanine show no additional peaks which could correspond to solvated amino acid ions. The spectra for serine, threonine, asparagine, lysine, methionine, histidine, arginine, and tryptophan show a secondary peak 18 m/z to the right of the unsolvated peak, corresponding to the singly hydrated amino acid ion. Leucine shows a third and possibly fourth peak corresponding to higher solvation states. The tryptophan spectrum shows peaks below 200 m/z that are consistent with hydrated states of the hydronium ion and that also appear in control measurements of aqueous solutions with no amino acid present. Tryptophan, which has a lower solubility than the other amino acids studied, produces a relatively weak signal. Four proteinogenic amino acids are absent from Fig. 2b: we do not attempt to measure Aspartic acid and glutamic acid in positive ion mode because of their low isoelectric points; we also ignore isoleucine because it is indistinguishable from leucine based on m/z, and tyrosine gave poor emission characteristics, likely related to its low solubility in water.

2.2 Measuring post-translationally modified peptides

Figure 2c shows mass spectra of glutathione and two chemically modified variants, s-nitrosoglutathione, and s-acetylglutathione. Glutathione is a tripeptide found in high concentrations in most cells [22], and the variants we studied result from common post-translational modifications. Ion sources with 20 nm inner diameter tips generate the peptide ions from 100 mM aqueous solutions with a pH between 3.1 and 3.9, adjusted by the addition of acetic acid. The glutathione spectrum shows a single peak at 307 m/z, which corresponds to the singly charged, unsolvated glutathione ion. The spectra of

s-acetylglutathione and s-nitrosoglutathione show dominant peaks at 349 m/z and 336 m/z, respectively, corresponding to the singly charged, unsolvated peptide ions; each spectrum also shows two progressively smaller peaks 18 and 36 m/z to the right of the dominant peak, corresponding to singly and doubly solvated peptide ions, respectively.

2.3 Ion transmission efficiency

We measure the efficiency with which ions pass from the nanopore source to a distant detector in a high vacuum environment as illustrated in Fig. 3a. Ions emitted by the source are focused into the 2 cm opening of a Faraday cup located $\sim$ 50 cm away. The ratio of the current collected by the Faraday cup, I_C, to I_T is the ion transmission efficiency. Figure 3b shows I_C, I_T, and the ion transmission efficiency measured over the course of a 17 minute-long experiment using a tip with a 39 nm inner diameter filled with a 100 mM aqueous solution of sodium iodide. The mean ion transmission efficiency is 93.4% $\pm$ 1.7%. Although I_T drifts between about 780 pA and 840 pA on a timescale of minutes, the slow rises and falls in I_T are mirrored by I_C, resulting in a relatively stable transmission efficiency.

2.4 Separating ions and charged droplets

We investigate the possibility that the nanopore source emits charged droplets in addition to ions by adding a magnetic sector to the flight path as shown in Fig. 3c. The 6 cm diameter, 0.54 T magnetic sector deflects charged species based on their mass-to-charge ratio. Droplets larger than 15 nm in diameter deflect by less than 3.1° and enter the Faraday cup, even if they are charged to

the Rayleigh limit [23, 24]. The Faraday cup measures the current from charged droplets, I_{Drop}. Meanwhile, ions with m/z in the range ~ 70 to ~ 325 deflect onto a separate Faraday plate and produce an ion current I_{Ion}. Figure 3d shows I_{Ion}, I_{Drop}, and the ionic fraction of the total measured current ($\frac{I_{\mathrm{Ion}}}{I_{\mathrm{Ion}}+I_{\mathrm{Drop}}}$) for a 2 minute-long measurement performed using a 28 nm inner diameter tip filled with a 100 mM aqueous solution of NaI. I_{Ion} rises from about 60 pA to about 80 pA while no I_{Drop} was observed. The nanopore source appears to emit only ions; however, this measurement cannot exclude the occurance of highly charged droplets smaller than about 15 nm.

2.5 Calculating the probability of ions scattering

Calculations indicate that most ions trace collisionless trajectories from the ion source to the detector. Figure 4 shows the probability that an amino acid ion dressed with a hydration shell collides with a gas molecule, based on the kinetic theory of gases. We assume that ions pass through a distribution of evaporating water molecules [25] and a homogeneous low-pressure background of N_2. Figure 4 sketches the physical situation and plots the number density of gas molecules and the cumulative collision probability as functions of the distance from the meniscus. The cumulative probability of an ion colliding with a gas molecule over the entire 50 cm trajectory from the source to the detector is just 2.1%, meaning the vast majority of ions do not experience any collisions. Most of the collisions occur within 200 nm of the liquid meniscus due to the high density of evaporated water molecules there. A detailed description of these calculations is found in the Supplemental Information.

3 Discussion

Two lines of evidence lead us to rule out the conventional, droplet-mediated electrospray mechanism (Fig. 1a) as the main source of ions that we measure. First, we measure no droplets larger than 10 nm among the charged species delivered by the source (Fig. 3d). Second, our instrument lacks the background gas that normally sustains the evaporation of water from droplets in an electrospray [4]. In high vacuum, nanoscale aqueous droplets shed only a small fraction of their mass before the evaporation process freezes up due to latent heat loss [26, 27]. Therefore, a sustained release of ions from droplets cannot occur in our instrument.

We can explain our findings with an alternative ion emission mechanism: the evaporation of ions directly from the liquid-vacuum interface at the nanopore, as illustrated in Fig. 1b. Ion evaporation is a thermal process by which ions escape from a liquid with assistance from a strong electric field at the surface [20]. A strong enough electric field typically arises when the ratio of the conductivity, K, to the flow rate, Q, of an electrified liquid is sufficiently large [28, 29]. Accordingly, previous studies have observed ion evaporation from highly conductive liquids such as liquid metals [30], ionic liquids [31], and concentrated electrolyte solutions in formamide [32]. The amino acid solutions we measured have relatively low conductivities (in the range 0.01-0.5 S/m), but the flow rate produced in a nanocapillary under 1 atm of applied pressure is exceptionally low (<10 pL/min) [17], so the resulting K/Q is still large. K/Q values for our experiments are of the same order as those reported for the ionic liquid EMI-BF_4 while exhibiting ion evaporation with no droplet emission [31]. Furthermore, the distributions of ion solvation states we measured in Fig. 1d and elsewhere are similar to the distributions measured by Luedtke et al. from

sodium iodide in formamide, which they also attributed to ion evaporation [33]. A few previous studies used similarly sized emitter tips to produce ions for MS, but a background gas was always used and the emission mechanism was presumed to be conventional ESI [34].

It is striking that we mostly measured bare ions, rather than hydrated ion clusters in Fig. 2c and d. Were the ions emitted in this bare state or were they emitted in a hydrated state and subsequently shed their hydration shell on the way to the detector? Because only about 2% of emitted ions would experience even a single collision (Fig. 4), we can rule out collisions with gas molecules as a mechanism for desolvating ion clusters. Furthermore, the tip size appears to influence the hydration state (Fig. 2a); this suggests that it is the local environment at the source that controls the hydration state rather than processes occurring in flight.

The high ion transmission efficiency (Fig. 3b) is a direct consequence of the nanopore ion source's emission mechanism. Ion evaporation transfers individual ions directly into a high vacuum environment where they neither collide with background gas molecules nor undergo coulomb explosions that would propel charged species in random directions. The trajectory of each ion emitted from the source is mainly determined by the electric fields that are shaped by the ion optics. With further optimization it is conceivable to achieve true single-molecule sensitivity.

In summary, we have demonstrated a nanopore ion source that emits amino acid and small peptide ions directly into high vacuum. The ability to emit bare ions, as opposed to solvated ion clusters or charged droplets, facilitates the identification of different amino acids and post-translational modifications. Ions evidently evaporate directly from the liquid meniscus at the tip, which

removes the need for a background gas to free ions from droplets. By doing away with background gas collisions and the need to transfer ions from ambient pressure to high vacuum, the nanopore ion source removes the primary modes of ion loss which are characteristic of electrospray ionization.

Methods

Preparing nanocapillaries

We pulled Nanocapillaries from 7.5 cm long quartz capillaries with 0.7 mm inner diameter and 1 mm outer diameter (QF100-70-7.5, Sutter Instruments) using a laser puller (P-2000, Sutter Instruments) according to the following single-line recipe: heat = 650, velocity = 45, delay = 175, pull = 190. Thermal evaporation (CED 030, BalTec) deposited approximately 5 nm of carbon to the nanocapillaries using double-stranded carbon thread (Leica Microsystems). We then imaged the nanocapillaries by scanning electron microscopy (LEO 1530 VP, Zeiss inc.) to measure the tip size. A plasma cleaner (Plasma Preen II-973, Plasmatic Systems Inc.) cleaned the pulled nanocapillaries in air for two minutes prior to their use.

Amino acid solutions

Amino acid solutions comprised the amino acid of interest (Sigma-aldrich) dissolved in deionized water (Millipore) at a concentration of 100 mM, with the exception of tryptophan, whose concentration concentration was 50 mM. The addition of 0.1-0.5% v/v glacial acetic acid (Sigma-Aldrich) reduced the pH below the amino acid's isoelectric point. Peptide solutions comprised the

peptide of interest (glutathione, s-acetylglutathione, or s-nitrosoglutathione) dissolved in deionized water at a concentration of 100 mM. We purchased glutathione and s-acetylglutathione in powder form (Sigma-aldrich), and synthesized S-nitrosoglutathione from glutathione according to a protocol from T.W. Hart [35]. We measured the pH and conductivities of each solution using a pH meter (Ultrabasic Benchtop, Denver Instruments) and conductivity meter (Sension+ EC71 GLP, Hach) respectively.

Delivering solutions to the ion source

A previously described tube-in-tube system delivers sample solution to the nanocapillary tip while flushing away old solution [21]. A 150 μm i.d., 360 μm o.d. PEEK tube (IDEX Health and Science) carries sample solution in while a wider (0.04" i.d., 1/16" o.d.) PEEK tube (IDEX Health and Science) carries used solution away from the tip around the outside of the thinner inner tube. We make Ag/AgCl electrodes by placing a length of silver wire in bleach for 15-20 minutes. Threading the Ag/AgCl electrode through the outer PEEK tubing allows us to apply a voltage to the solution at the tip of the ion source. A syringe pump (NE-300, New Era Pump Systems) supplies fresh solution to the ion source through the inner PEEK tubing. A VacuTight upchurch fitting (IDEX Health and Science) creates a seal around the base of the nanocapillary and end of the outer tube to prevent the solution from leaking into the vacuum. A 1/4" diameter steel tube houses the tube-in-tube system, and enters the vacuum chamber of the mass spectrometer through a KF-40 to Quick-Connect adapter (Lesker Vacuum) .

Amino acid and glutathione measurements

The instrument used for all the amino acid and peptide measurements presented in this work is a custom-built quadrupole mass spectrometer fully described by Bush et al [21]. The instrument comprises a custom einzel lens, a quadrupole mass filter (QC MAX-500, Extrel inc.), an ion bender (Extrel inc.), and a channel electron multiplier detector with a conversion dynode (DeTech 413), which is sensitive to single ions. The base pressure of the instrument is 10^{-8} torr. When a nanopore ion source is introduced into the mass spectrometer the pressure typically rises to $10^{-7} - 10^{-6}$ torr.

We prefilled the nanocapillaries with the amino acid or peptide solution using a microfil flexible needle (World Precision Instruments) before inserting them into the mass spectrometer. The tube-in-tube system continuously refreshed the solution at the tip by pumping solution through the inner tubing from a syringe pump (NE-300, New Era Pump Systems) at a rate of 0.4 mL/hour. A voltage of +100 V was applied to the electrode inside the capillary using a high voltage source measure unit (2657A, Keithley Instruments) while a negative voltage was slowly applied to the extraction electrode using a high voltage power supply (Bertan 230, Spellman HV) until ionization was observed. The onset of emission typically occurred when the total extraction voltage was between 200 and 350 V.

3.1 Ion transmission efficiency measurements

We carried out measurements of ion transmission in a custom vacuum chamber containing ion optics and a Faraday cup (Fig. 3a). A high voltage source-measure unit (2410, Keithley Instruments) measures the emission current while also applying a high voltage to the tip via the Ag/AgCl electrode. We measured the leakage current through the BNC cable connecting the source-measure unit to the tip to be 100 pA, this value was then subtracted off of the measured emission current. A current-preamplifier (SR570, Stanford Research Systems) measured the current striking the Faraday cup and connected to a DAQ card (NI PCIe-6251 National instruments). An 8-channel high-voltage power supply (DT8033, CAEN) supplied voltages to the ion optics. A custom Labview (National Instruments) program controlled the voltage applied to the tip and recorded the emitted and transmitted currents.

3.2 Magnetic sector measurements

We constructed a basic magnetic sector mass spectrometer by adding a magnet and a Faraday plate to the vacuum chamber described above. The magnet consisted of a neodymium magnet with a yoke constructed from low-carbon magnetic iron (ASTM A848). The yoke concentrates the field in a flat circular region, 6 cm in diameter and 1 cm in height, which was placed directly downstream of the ion optics. We measured the field strength within the flat circular region to be $B = 0.54 \pm 0.02$ T using a magnetometer. The Faraday plate is a stainless steel disk, 5 inches in diameter, and 0.02" thick, connected directly to an electrical feedthrough by a steel wire. The Faraday plate was mounted at 45° relative to the Faraday cup, at the same distance from the center of the

magnetic sector. A source-measure unit (2410, Keithley Instruments) measured the current emitted from the tip, and two separate SR570 current pre-amplifier (Stanford Research Systems) measured the ion and droplet currents striking the Faraday plate and cup respectively.

Data availability statement

The data that support the findings of this study are available from the corresponding author upon request.

References

[1] Aebersold, R. & Mann, M. Mass-spectrometric exploration of proteome structure and function. *Nature* **537** (7620), 347–355 (2016) .

[2] Cole, R. B. *Electrospray and MALDI mass spectrometry: fundamentals, instrumentation, practicalities, and biological applications* (John Wiley & Sons, 2011).

[3] Taylor, G. I. Electrically driven jets. *Proceedings of the Royal Society of London. A. Mathematical and Physical Sciences* **313** (1515), 453–475 (1969) .

[4] Kebarle, P. & Verkerk, U. H. Electrospray: from ions in solution to ions in the gas phase, what we know now. *Mass spectrometry reviews* **28** (6), 898–917 (2009) .

[5] Smith, R. D., Loo, J. A., Edmonds, C. G., Barinaga, C. J. & Udseth, H. R. New developments in biochemical mass spectrometry: electrospray

ionization. *Analytical chemistry* **62** (9), 882–899 (1990) .

[6] Wilm, M. & Mann, M. Analytical properties of the nanoelectrospray ion source. *Analytical chemistry* **68** (1), 1–8 (1996) .

[7] El-Faramawy, A., Siu, K. M. & Thomson, B. A. Efficiency of nano-electrospray ionization. *Journal of the American Society for Mass Spectrometry* **16** (10), 1702–1707 (2005) .

[8] Hawkridge, A. M. Practical considerations and current limitations in quantitative mass spectrometry-based proteomics (2014) .

[9] Marginean, I., Page, J. S., Tolmachev, A. V., Tang, K. & Smith, R. D. Achieving 50% ionization efficiency in subambient pressure ionization with nanoelectrospray. *Analytical chemistry* **82** (22), 9344–9349 (2010) .

[10] Tang, K. & Smith, R. D. Physical/chemical separations in the break-up of highly charged droplets from electrosprays. *Journal of the American Society for Mass Spectrometry* **12** (3), 343–347 (2001) .

[11] Li, S. *et al.* An integrated platform for isolation, processing, and mass spectrometry-based proteomic profiling of rare cells in whole blood*[s]. *Molecular & Cellular Proteomics* **14** (6), 1672–1683 (2015) .

[12] Callahan, N., Tullman, J., Kelman, Z. & Marino, J. Strategies for development of a next-generation protein sequencing platform. *Trends in biochemical sciences* **45** (1), 76–89 (2020) .

[13] Kelly, R. T. Single-cell proteomics: progress and prospects. *Molecular & Cellular Proteomics* **19** (11), 1739–1748 (2020) .

[14] Restrepo-Pérez, L., Joo, C. & Dekker, C. Paving the way to single-molecule protein sequencing. *Nature Nanotechnology* **13** (9), 786–796 (2018). URL https://doi.org/10.1038/s41565-018-0236-6. https://doi.org/10.1038/s41565-018-0236-6 .

[15] Alfaro, J. A. *et al.* The emerging landscape of single-molecule protein sequencing technologies. *Nature methods* **18** (6), 604–617 (2021) .

[16] Steinbock, L. J., Otto, O., Chimerel, C., Gornall, J. & Keyser, U. F. Detecting dna folding with nanocapillaries. *Nano letters* **10** (7), 2493–2497 (2010) .

[17] Maulbetsch, W. *Nanopore Mass Spectrometry.* Ph.D. thesis, Brown University (2018). URL https://repository.library.brown.edu/studio/item/bdr:792908/.

[18] Higuera, F. Qualitative analysis of the minimum flow rate of a cone-jet of a very polar liquid. *Journal of Fluid Mechanics* **816**, 428–441 (2017) .

[19] Higuera, F. Model of the meniscus of an ionic-liquid ion source. *Physical Review E* **77** (2), 026308 (2008) .

[20] Iribarne, J. V. & Thomson, B. A. On the evaporation of small ions from charged droplets. *The Journal of Chemical Physics* **64** (6), 2287–2294 (1976). URL https://aip.scitation.org/doi/abs/10.1063/1.432536. https://doi.org/10.1063/1.432536, https://arxiv.org/abs/https://aip.scitation.org/doi/pdf/10.1063/1.432536 .

[21] Bush, J. *et al.* The nanopore mass spectrometer. *Review of Scientific Instruments* **88** (11), 113307 (2017) .

[22] Meister, A. & Anderson, M. E. Glutathione. *Annual review of biochemistry* **52** (1), 711–760 (1983) .

[23] Rayleigh, L. Xx. on the equilibrium of liquid conducting masses charged with electricity. *The London, Edinburgh, and Dublin Philosophical Magazine and Journal of Science* **14** (87), 184–186 (1882) .

[24] Taflin, D. C., Ward, T. L. & Davis, E. J. Electrified droplet fission and the rayleigh limit. *Langmuir* **5** (2), 376–384 (1989) .

[25] Smith, J. D., Cappa, C. D., Drisdell, W. S., Cohen, R. C. & Saykally, R. J. Raman thermometry measurements of free evaporation from liquid water droplets. *Journal of the American Chemical Society* **128** (39), 12892–12898 (2006) .

[26] Caleman, C. & van der Spoel, D. Temperature and structural changes of water clusters in vacuum due to evaporation. *The Journal of chemical physics* **125** (15), 154508 (2006) .

[27] Sellberg, J. A. *et al.* Ultrafast x-ray probing of water structure below the homogeneous ice nucleation temperature. *Nature* **510** (7505), 381–384 (2014) .

[28] Guerrero, I., Bocanegra, R., Higuera, F. & De La Mora, J. F. Ion evaporation from taylor cones of propylene carbonate mixed with ionic liquids. *Journal of Fluid Mechanics* **591**, 437–459 (2007) .

[29] Romero-Sanz, I., Bocanegra, R., Fernandez De La Mora, J. & Gamero-Castano, M. Source of heavy molecular ions based on taylor cones of ionic liquids operating in the pure ion evaporation regime. *Journal of Applied Physics* **94** (5), 3599–3605 (2003) .

[30] Prewett, P. D., Mair, G. L. R. & Thompson, S. P. Some comments on the mechanism of emission from liquid metal ion sources. *Journal of Physics D: Applied Physics* **15** (7), 1339–1348 (1982). https://doi.org/10.1088/0022-3727/15/7/027 .

[31] Romero-Sanz, I., Bocanegra, R., Fernandez de la Mora, J. & Gamero-Castaño, M. Source of heavy molecular ions based on taylor cones of ionic liquids operating in the pure ion evaporation regime. *Journal of Applied Physics* **94** (5), 3599–3605 (2003). URL https://doi.org/10.1063/1.1598281. https://doi.org/10.1063/1.1598281, https://arxiv.org/abs/https://doi.org/10.1063/1.1598281 .

[32] Gamero-Castano, M. Electric-field-induced ion evaporation from dielectric liquid. *Physical review letters* **89** (14), 147602 (2002) .

[33] Luedtke, W. *et al.* Nanojets, electrospray, and ion field evaporation: Molecular dynamics simulations and laboratory experiments. *The Journal of Physical Chemistry A* **112** (40), 9628–9649 (2008) .

[34] Yuill, E. M., Sa, N., Ray, S. J., Hieftje, G. M. & Baker, L. A. Electrospray ionization from nanopipette emitters with tip diameters of less than 100 nm. *Analytical chemistry* **85** (18), 8498–8502 (2013) .

[35] Hart, T. W. Some observations concerning the s-nitroso and s-phenylsulphonyl derivatives of l-cysteine and glutathione. *Tetrahedron Letters* **26** (16), 2013–2016 (1985) .

Acknowledgements

We thank Oxford Nanopore Technologies LTD. for supporting this work. Aspects of this work were also supported by the Institute for Molecular and Nanoscale Innovation at Brown University. N.D. was partially supported by the Brown IMSD program (NIH R25GM083270) and Graduate Fellowships for STEM Diversity (GFSD). H.S. was partially supported by the Brown UTRA program. B.W. was partially supported by NSF 1409577.

Competing Interests Statement

D.S. declares a competing interest in Oxford Nanopore Technologies, Ltd.

Author Contributions

Conceptualization & supervision: D.S.; Research design: D.S., M.L., W.M.; Mass spectrometry measurements: M.L., N.D., and H.S.; Ion source characterization: N.D., W.M., and B.W.; Manuscript writing and editing: N.D. and D.S.; Figure preparation: N.D.; Funding acquisition: D.S.; All authors contributed to the discussions.

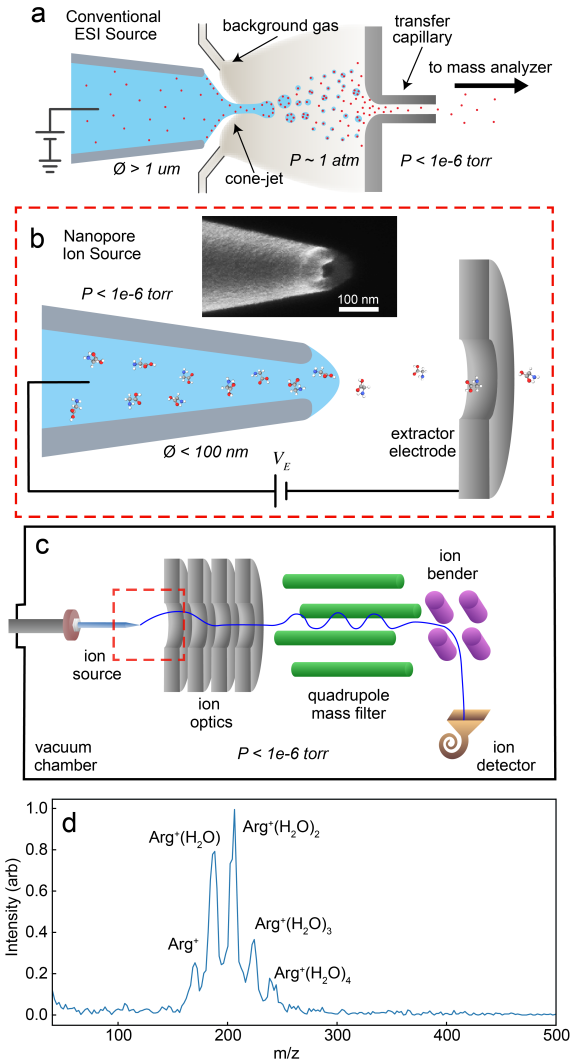

Fig. 1 Comparison of conventional electrospray ion source with nanopore ion source. a, Schematic of conventional electrospray ionization highlighting the background gas that stimulates evaporation of solvent from droplets and the transfer capillary where significant ion loss occurs. **b**, Schematic of a nanopore ion source showing the liquid-filled nanocapillary tip, the extractor electrode, and the extraction voltage V_e applied between them. Inset shows an SEM image of the tip of a pulled quartz nanocapillary with a tip inner diameter of 30 nm. **c**, Schematic of the mass spectrometer used in this study. Ion optics comprising an extractor electrode and an einzel lens extract ions from the liquid meniscus at the ion source and focus them through a quadrupole mass filter and an electrostatic ion bender. The transmitted ions strike a channel electron multiplier detector which is sensitive to single ions. **d**, Mass spectrum of 100 mM arginine in aqueous solution obtained with a 41 nm inner diameter nanopore ion source in our quadrupole mass spectrometer.

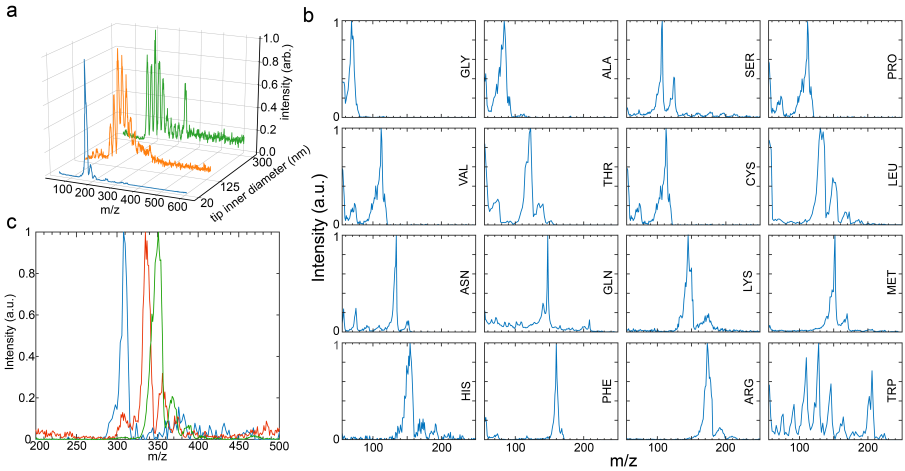

Fig. 2 Amino acid and peptide spectra. a, Mass spectrum of 100mM arginine solution in H_2O using nanopore ion sources with 3 different inner tip diameters (20 nm, 125 nm, and 300 nm). **b**, Gallery of 16 amino acid mass spectra, ordered from top left to bottom right by mass. All experiments were carried out using nanocapillaries with 20-60 nm inner tip diameters. **v**, Overlaid mass spectra of glutathione (blue) and two of it's PTM variants, s-nitrosoglutathione (green) and s-acetylglutathione (red).

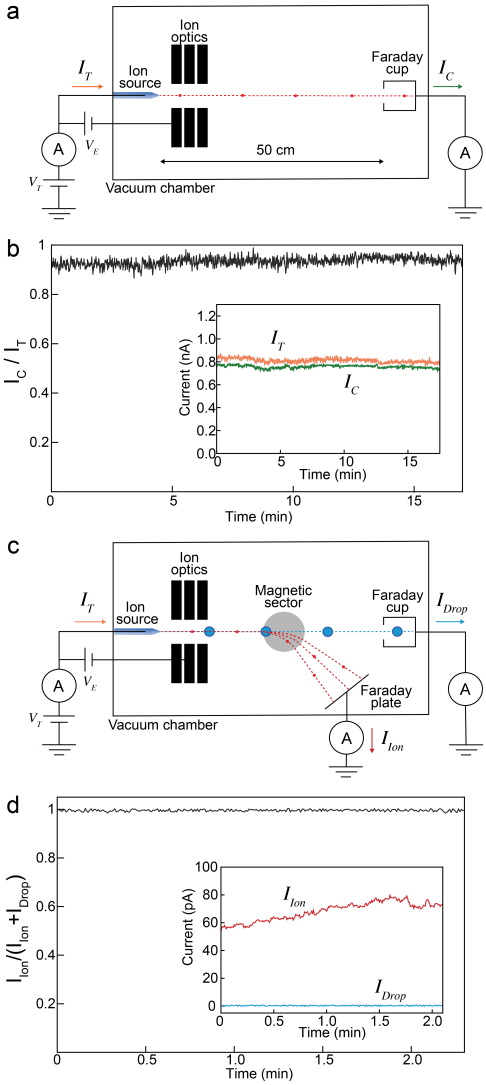

Fig. 3 Ion transmission efficiency and ion/droplet current fractions. a, Experimental setup to measure the ion transmission efficiency of the nanopore ion source. A voltage V_T is applied to the nanopore ion source by a source-measure unit to produce the tip current I_T. The emitted ions are focused by the ion optics and strike the Faraday cup where the collected current I_C is measured by a current-to-voltage preamplifier. The experiment is carried out inside a vacuum chamber at pressures of around 10^{-7} torr. **b**, Plot of the ion transmission efficiency measured over several minutes from a nanopore ion source using 100 mM NaI in water. The inset shows I_T (orange line) and I_C (green line) plotted over the same time period. **c**, Experimental setup used to measure the relative fraction of ion current, I_{Ion}, and droplet current, I_{Drop}. A magnetic sector (diameter = 6 cm,$B = 0.54$ T) is placed past the ion optics to deflect emitted particles by their mass-to-charge ratio. I_{Ion} is collected by a wide Faraday plate and I_{Drop} is collected by the Faraday cup. The centers of the Faraday cup and Faraday plate are equidistant from the center of the magnetic sector and separated by 45°. **d**, A plot of the fraction I_{ion} makes up of the total detected current ($I_{Ion} + I_{Drop}$) over 2 minutes using 100 mM NaI in water. The inset plots I_{Ion} and I_{Drop} over the same time period.

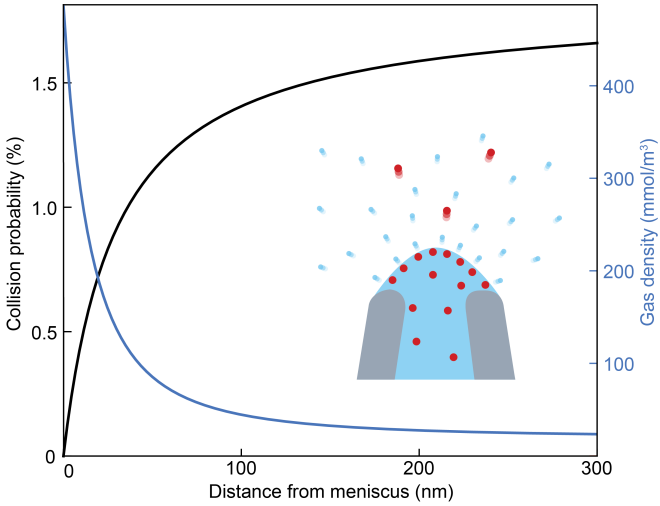

Fig. 4 Ion collision probability. The black curve is the cumulative probability that an emitted amino acid with a small hydration shell (radius = 7 Å) will collide with an evaporated water molecule or background N_2 molecule as a function of distance from the meniscus, r. The blue curve shows the calculated maximum water vapor density as a function of the distance from the meniscus. We conservatively assumed that the vapor pressure on the vacuum side of the meniscus is 8.75 torr, half the equilibrium vapor pressure of water at room temperature. The inset shows a schematic representation of the distribution of evaporating water molecules near the meniscus.